Original Article

Evaluating thermal stability of rare-earth containing wasteforms at extraordinary nuclear disposal conditions

Miae Kim [a, b], Kyong-Soo Hong [b], Jaeyoung Lee [b], Mirang Byeon [b], Yesul Jeong [b], Jong Hwa Kim [c], Wooyong Um [a, **], Hyun Gyu Kim [b, *]

[a] Division of Advanced Nuclear Engineering, Pohang University of Science and Technology, Pohang, 37673, South Korea
[b] Busan Centre, Korea Basic Science Institute, Busan, 46742, South Korea
[c] Daegu Centre, Korea Basic Science Institute, Daegu, 41566, South Korea

ABSTRACT

The thermal stability and crystallization behaviors of La_2O_3 containing B_2O_3-CaO−Al_2O_3 glass waste forms were investigated to evaluate the stability of waste form during emergencies in deep geological disposal. For glasses containing 15% La_2O_3, $LaBO_3$ phases were observed as major crystals from 780 °C and exhibited needlelike structures. Al, Ca, and O were homogeneously distributed throughout the entire specimen, while some portions of B and La were concentrated in some parts. By differential thermal analysis at various heating rates, the activation energy for grain growth and the crystallization rate of $LaBO_3$ were calculated to be 12.6 kJ/mol and 199.5 kJ/mol, respectively. These values are comparable to other waste forms being developed for the same purpose.

© 2021 Korean Nuclear Society, Published by Elsevier Korea LLC. This is an open access article under the CC BY-NC-ND license (http://creativecommons.org/licenses/by-nc-nd/4.0/).

1. Introduction

Over the past decades, various types of wastes have been generated from nuclear power dismantling and dissecting power stations and reprocessing spent nuclear fuels (in which spent nuclear fuels are reused or recycled into next-generation reactor systems) [1,2]. Among these, lanthanides are directly generated from reprocessing and usually used in immobilization techniques and as surrogate materials for actinides [3,4]. The volume of lanthanide wastes obtained from reprocessing and pyroprocessing are relatively high [5]. Therefore, lanthanide waste forms have gained increasing attention [6−8].

B_2O_3-CaO-Al_2O_3 glass systems were developed to immobilize lanthanide oxides generated from pyroprocessing [9,10]. These waste forms are processable and durable and help maximize waste loading [9]. In particular, they exhibited good chemical durability when a standard leaching test was performed at 90 °C. However, thermal stability and crystallization behaviors of waste forms have rarely been studied. The ambient temperature in deep geological repositories under normal conditions, which does not exceed ~150 °C [11,12], is difficult to estimate during accidents [13]. Therefore, we investigated the crystal formation behaviors by applying additional heat treatment up to 900 °C [14].

Crystallization could occur when the glasses are exposed to high-temperature conditions. The impact of crystallization on glassy waste forms cannot be concluded as good or bad [15]. We attempted to crystallize glassy waste forms intentionally and fabricate glass-ceramic waste forms to enhance their mechanical properties [16] or partitioning effect [17]. Alternatively, once uncontrolled crystallization occurs, the properties of waste forms may deteriorate drastically [18]. Therefore, we need to consider how uncontrolled crystallization can occur relatively easily by calculating the activation energy for crystallization of the glass. Furthermore, additional bonds being formed during crystallization between radioactive nuclides (La) and the matrix former (B) can delay the release of target nuclides (from the glass phase) and help enhance safety and stability.

In this study, we attempted to fabricate the B_2O_3−CaO−Al_2O_3 glasses containing La_2O_3, determine the formation behaviors or morphological characteristics of crystalline phases by heat treatment at various temperatures, and assess the thermal stability and

---

* Corresponding author.
** Corresponding author.
E-mail addresses: wooyongum@postech.ac.kr (W. Um), hhgkim@kbsi.re.kr (H.G. Kim).

crystallization kinetics by thermal analysis at various heating rates.

2. Experimental procedures

We fabricated a B_2O_3—CaO—Al_2O_3 glass system containing 0—15 mol% of La_2O_3 using nominal composition, as shown in Table 1. A glass batch of approximately 20 g was prepared by mixing commercial powders of reagent B_2O_3 (Sigma-Aldrich, 99.99%), CaO (Sigma-Aldrich, 99.9%), and Al_2O_3 (Sigma-Aldrich, 99.99%).

The raw materials contained in a platinum crucible were melted at 1300 °C for 30 min in an atmosphere electric furnace. The liquid was poured onto an iron plate and pressed quickly with another iron plate with a thickness of approximately 2 mm. The obtained glasses were labeled as La0, La6, La9, and La15 based on the content of La_2O_3. The maximum La_2O_3 composition of 15 mol % were determined as the composition without crystallization just after quenching under our glass melting condition.

The density (ρ, g/cm^3) for all specimens was measured using a density measuring kit (MS-DNY-52, Mettler Toledo) and the Archimedes method (with deionized water as the liquid medium) at room temperature. All measurements for each specimen were performed thrice and averaged. The molar volume (V_m, cm^3/mol) was calculated from the density and molar weight of the samples.

We continued to determine the crystallization kinetics only for the La15 specimens with the highest density. The crystallization temperature (T_x) was determined using a differential thermal analyzer (DTA, TA Q600, Pusan Center) for La15 with heating rates of 7, 10, 15, and 20 °C/min in the temperature range between 200 °C and 1000 °C in air flux.

We additionally heat-treated the La15 samples from 680 °C to 900 °C at intervals of 20 °C for 3 h. The specimens were ground and sieved, then all the powder size we used were less than 45 μm. X-ray diffraction patterns for each heat-treated specimen were recorded using Cu-Ka (λ = 0.15418 nm) radiation at 40 kV and 100 mA (for 2θ = 10°—80°). For each heat-treated specimen, we used a scanning electron microscope (SEM, Hitachi, SU70) to obtain the morphology of the formed crystalline phases. In addition, we used a transmission electron microscope (TEM, JEOL, JEM-2100F) to reveal the detailed morphological behavior of a crystallized specimen. They were operated at an accelerating voltage of 200 kV at the Daegu Center of the Korea Basic Science Institute (KBSI). Prior to analysis, the samples were sonicated for 2 h and dispersed in ethanol, and the solutions were dropped onto a porous carbon film on a copper grid. Next, the samples were air-dried, and energy dispersive spectroscopic analysis was subsequently performed.

3. Results and discussion

3.1. Basic characteristics of different La_2O_3-containing glass systems

Fig. 1 represents the appearance of the fabricated glasses with various La_2O_3 concentrations (0—15%) in B_2O_3—CaO—Al_2O_3 glass system. All glasses were homogeneous and transparent. The influence of the added La_2O_3 on the appearance was not significant.
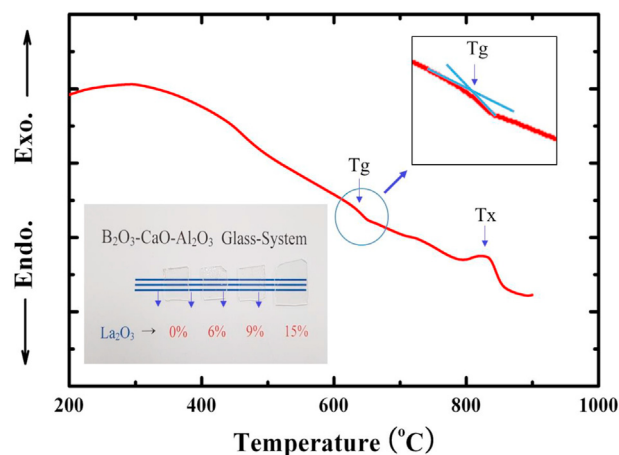

Fig. 1. DTA pattern of La15 specimen with a 10 °C/min heating rate. Inset: photographs of La0, La6, La9, and La15.

We measured the density (ρ, g/cm^3) and molar volume (V_m, cm^3/mol) of these glasses. The values are listed in Table 2. As the content of La_2O_3 increases, ρ and V_m increase. For the La15 specimen, 31% of ρ and 16% of V_m rise sharply compared to La0. These results are natural because of the high density of La_2O_3 compared to the other chemicals. The increase in molar volume can be because the increase in molecular weight due to the addition of La_2O_3 is larger than the increase in density.

From the perspective of volume reduction, materials with higher density are more economically advantageous as wasteforms because they can occupy only smaller portion of expensive disposal room. Therefore, we selected the specimen with the highest density and continued to investigate its thermal and crystallization behaviors. Fig. 1 shows the DTA pattern measured with a 10 °C/min heating rate for La15. We determined the glass transition temperature (T_g) at 642 °C and crystallization temperature (T_x) at 824 °C. To obtain information about the crystallization behavior of the La_2O_3-contaning B_2O_3—CaO—Al_2O_3 glass system, we selected the lowest heating temperature to be lower than the onset of the T_x. That is, the glasses were additionally heat-treated between 680 °C and 900 °C at intervals of 20 °C for 3 h.

3.2. Crystallization and structural behavior

Fig. 2 represents the X-ray diffraction patterns obtained from the heat-treated La15 at various temperatures. Based on these patterns, we could not find crystalline peaks up to 760 °C. From 780 °C, the peaks matched with lanthanum borate ($LaBO_3$, PDF#: 12—0762) crystal; orthorhombic structure, Pnam, cell parameter of 0.587 × 0.826 × 0.511 nm, and 90 × 90 × 90 °C. In addition, at this temperature, the specimens started to lose their transparency and turned pale white. T_x is the temperature at the maximum point of the exothermic peak obtained from the DTA [19] and not the starting point. Then, even at temperatures lower than the exact T_x,

Table 1
Nominal compositions (wt%) of B_2O_3—CaO—Al_2O_3 glasses containing various concentrations of La_2O_3.

	La0	La6	La9	La15
B_2O_3	56.2	52.9	51.2	47.8
CaO	25	23.5	22.7	21.3
Al_2O_3	18.8	17.6	17.1	15.9
La_2O_3	0	6	9	15
Total	100	100	100	100

Table 2
The density, ρ (g/cm^3), and molar volume, V_m (cm^3/mol), of B_2O_3—CaO—Al_2O_3—La_2O_3 glasses.

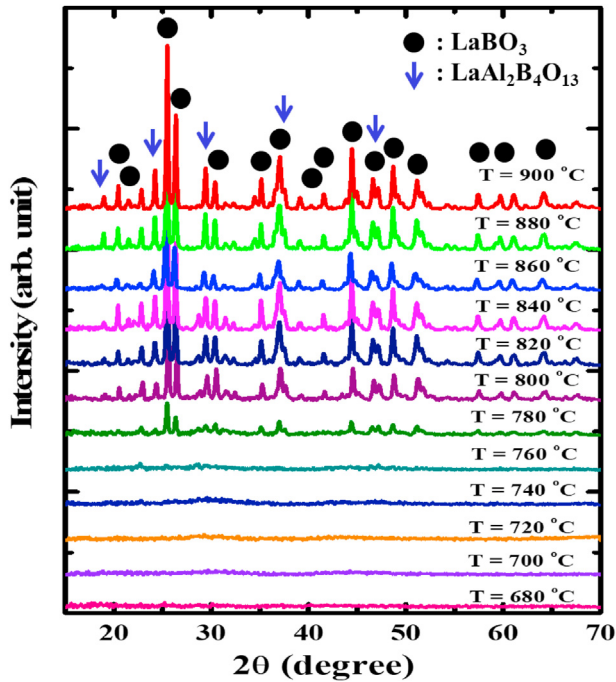| Composition	ρ (g/cm^3)	V_m (cm^3/mol)
La0	2.65 (±0.11)	27.28 (±1.18)
La6	2.93 (±0.07)	29.86 (±0.73)
La9	3.05 (±0.09)	31.19 (±0.89)
La15	3.48 (±0.07)	31.69 (±0.65)

Fig. 2. X-ray diffraction patterns obtained from the heat-treated La15 specimens from 680 °C to 900 °C at intervals of 20 °C for 3 h.

Fig. 4. Transmission electron micrograph of a powdery La15 specimen after heat treatment at 780 °C for 3 h glass and crystalline phases appeared. Inset: distance between planes in the crystalline phase.

that is on the onset of the T_x, crystallization can occur, as shown in Fig. 2. From 800 °C, an additional crystalline phase occurs; a lanthanum aluminum boron oxide crystal, $LaAl_2B_4O_{13}$, PDF#: 87-0484, hexagonal, P-62m, cell parameter: $0.461 \times 0.461 \times 0.935$ nm, $90 \times 90 \times 120$ °C. The abundance of the second crystalline phase was less than 20% of the total crystalline phases according to the compared intensities between the highest peaks of the two phases. Therefore, we estimate the major crystalline phase as a $LaBO_3$ crystal.

Fig. 3 shows the elemental distributions of a powdery specimen after heat treatment at 780 °C for 3 h. All the elements (Al, B, Ca, La, and O) existed in the powdery specimen. Al, Ca, and O were homogeneously distributed throughout the entire specimen, while
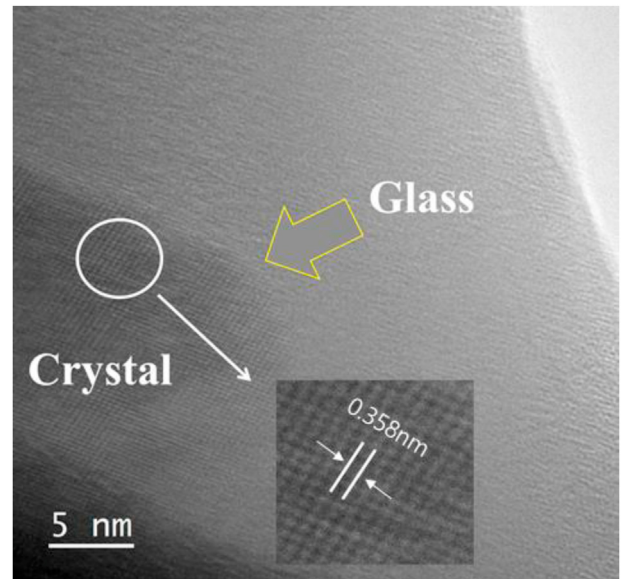
some portions of B and La were concentrated in some parts of the powder. This concentration could be due to the formation of $LaBO_3$ crystals inside the glassy phase. In addition, the formation of the crystal was confirmed again using the TEM data in Fig. 4. The crystalline phase was clearly distinguished from the amorphous glassy phase. The distance between the two planes of the crystals were 0.358 nm, which corresponds to the information of $LaBO_3$ [20].

3.3. Morphologic behaviors

To investigate the morphology of the crystals, we measured SEM images of all heat-treated specimens (Fig. 5). The homogenous surface in the specimen heat-treated at 680 °C changed gradually, forming needlelike crystals at 700 °C. These shapes were matched that of the previously observed $LaBO_3$ crystals [21]. As the
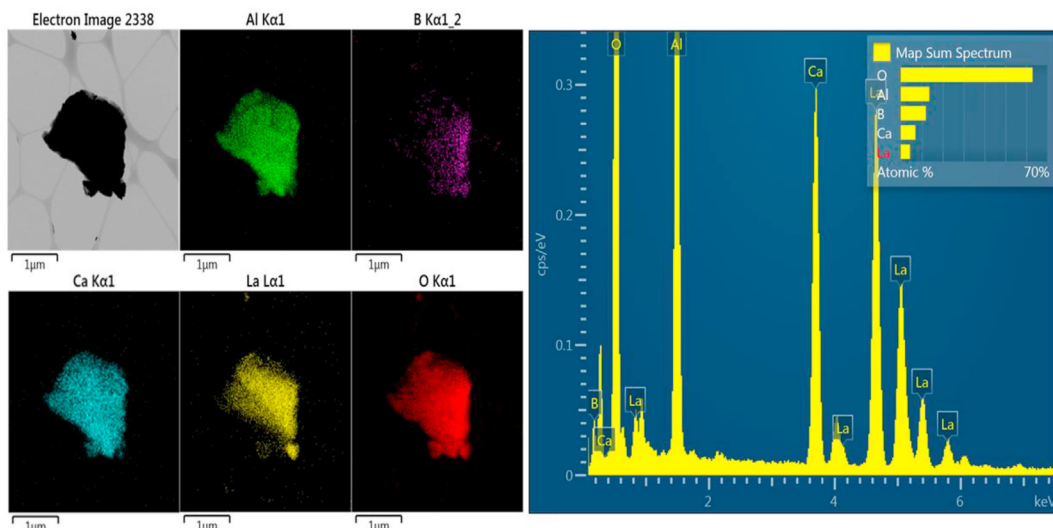

Fig. 3. Elemental mapping and spectrum of concentration of Al, B, Ca, La and O of a powdery La15 specimen after heat treatment at 780 °C for 3 h.
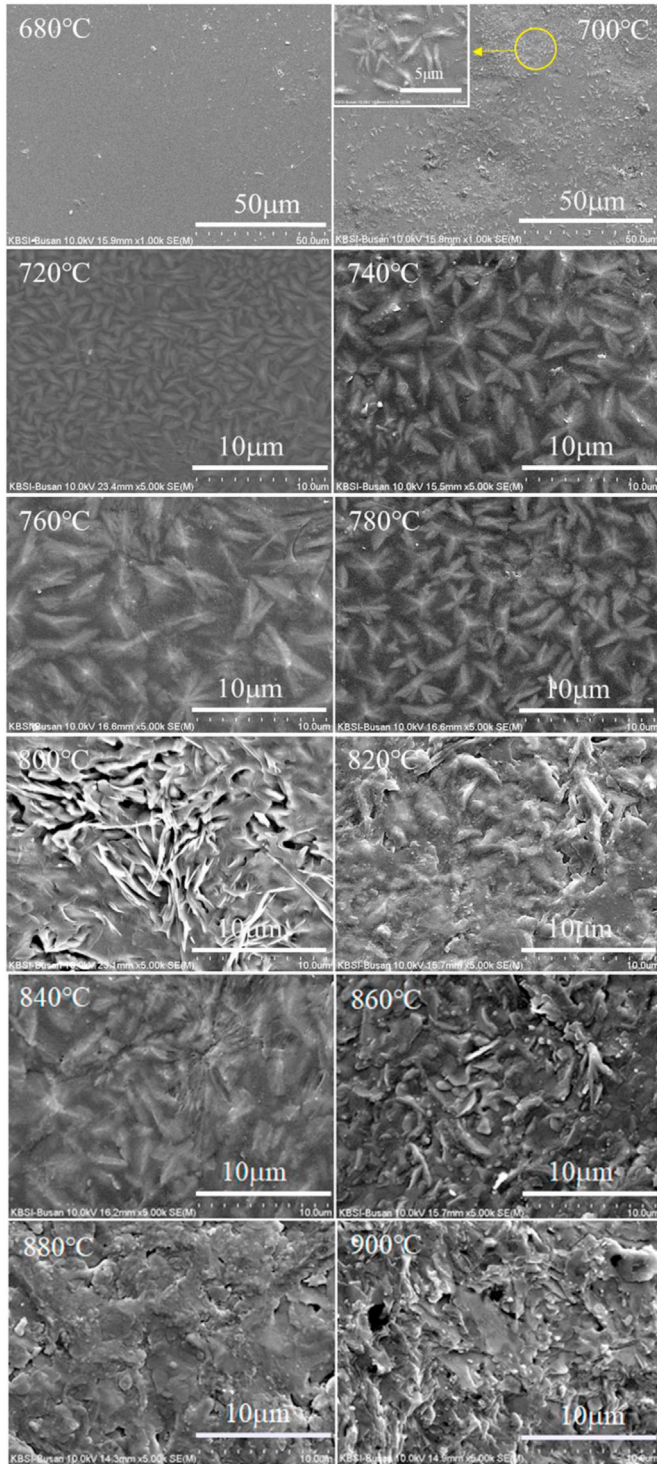
Fig. 5. Scanning electron micrographs SEM images of the heat-treated La15 specimens from 680 °C to 900 °C at intervals of 20 °C for 3 h.

temperature increased to 780 °C, the size of the crystals increased and the proportion of glassy phases decreased. At 800 °C, the crystals were tabular and flaky. Surface roughness (along with the flaky characteristics) seems to be reinforced as the heat treatment was applied at higher temperatures between 800 °C and 900 °C, and more interlocking grain patterns were observed.
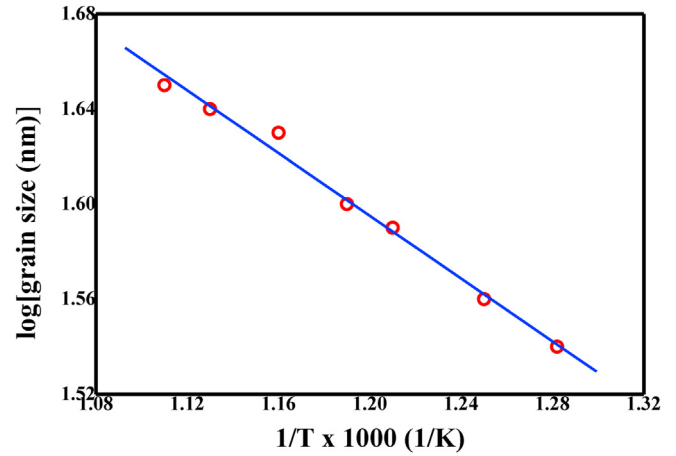

Fig. 6. Plot of log (grain size of $LaBO_3$ crystalline phases formed in heat-treated La15 glass at various temperature) versus the reciprocal of absolute temperature, 1/T.

3.4. Thermal and kinetic analyses

The size of the particles (L, nm) in La15 was estimated from the full width at half maximum (FWHM) of the XRD peak using Scherrer's equation [22];

$$L = 0.9\, \lambda\, /\, B \cos\theta \qquad (1)$$

where λ is the wavelength of the X-ray radiation ($\lambda = 0.154$ nm), B is the FWHM of the peak (radians) corrected for instrumental broadening, and θ is the Bragg angle. We calculated the estimated average particle size of these glass-ceramic systems as 48 nm. According to Coble's theory [23], the activation energy (E_g) of grain growth can be obtained by the Arrhenius equation [24]:

$$\mathrm{d}\ln k / \mathrm{d}T = E_g / RT^2 \qquad (2)$$

where k is the specific reaction rate constant, T is the absolute temperature, and R is the ideal gas constant. Jarcho et al. [25] revealed that the value of k was directly related to the grain size. By modifying and integrating Eq. (2), the following correlation is obtained:

$$\log D = (-E_g\, /\, 2.303\, R)/T + A \qquad (3)$$

where D is the grain size and A is the intercept. We drew a plot of log D versus the reciprocal of T and obtained a straight line, as shown in Fig. 6. The slope of the line represents the activation energy (E_g) of grain growth of the crystalline phase of $LaBO_3$ in this glass, and the value was 12.6 kJ/mol.

To calculate the activation energy of crystallization (E_c) of the $LaBO_3$ phase in La15, we measured the DTA spectra of the specimen at various heating rates (7 °C, 10 °C, 15 °C, and 20 °C), as shown in Fig. 7. T_x increased from 815 °C to 860 °C as the heating rate increased from 7 °C to 20 °C. This can be explained by the fact that at a slow heating rate, the glass state has sufficient time to transform into its crystalline phase. We applied the T_x values to the Kissinger's or Redhead's equation [26,27], as follows:

$$\ln\left(\Phi/T_x^2\right) = -E_c/RT_x + \text{const.} \qquad (4)$$

where Φ is the heating rate, T_x is the crystallization temperature or exothermic peak temperature, and R is the ideal gas constant. We obtained a straight line from the plot of $\ln\left(\Phi/T_x^2\right)$ vs. ($1000/T_x$), as shown in Fig. 8. By calculating the slope of the straight line, E_c was
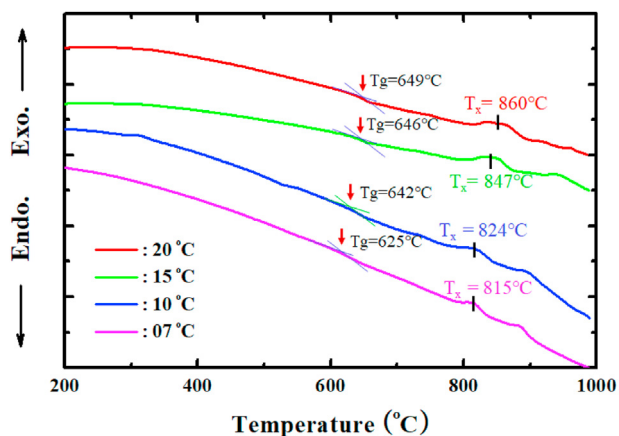
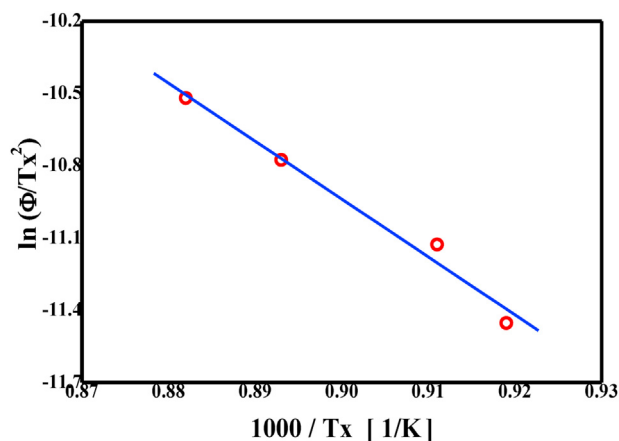**Fig. 7.** Differential thermal analysis of La15 specimen at various heating rates (7, 10, 15 and 20 °C/min).

Fig. 8. Plot of log (heating rate divided by square of the crystallization temperature) versus the reciprocal of crystallization temperature. The activation energy of transformation from amorphous to crystalline phase in La15 obtained from the plot.

Al, Ca, and O were homogeneously distributed throughout the entire specimen, while a few portions of B and La were concentrated in some parts measured by transmission electron microscopy and energy dispersive spectroscopy. By differential thermal analysis at various heating rates, the activation energy of grain growth of the $LaBO_3$ crystalline phase in this glass was 12.6 kJ/mol and the activation energy of crystallization was 199.5 kJ/mol. These values are comparable to those of other waste forms developed for the same purpose. We conclude that the waste forms are thermally stable (even at temperatures exceeding 900 °C).

Data availability

The raw data required to reproduce these findings are available to download from [https://dx.doi.org/10.17632/kn8p72k3db.1]. The processed data required to reproduce these findings are available to download from [https://dx.doi.org/10.17632/kn8p72k3db.1].

Declaration of competing interest

The authors declare that they have no known competing financial interests or personal relationships that could have appeared to influence the work reported in this paper.

Acknowledgement

Appendix A. Supplementary data

Supplementary data to this article can be found online at https://doi.org/10.1016/j.net.2021.02.025.

References

[1] M.I. Ojovan, W.E. Lee, S.N. Kalmykov, An Introduction to Nuclear Waste Immobilisation, Elsevier, 2019.
[2] C. Bayliss, K. Langley, Nuclear Decommissioning, Waste Management, and Environmental Site Remediation, Elsevier, 2003.
[3] R.C. Ewing, Nuclear waste forms for actinides, Proc. Natl. Acad. Sci. Unit. States Am. 96 (1999) 3432–3439, https://doi.org/10.1073/pnas.96.7.3432.
[4] P. Loiseau, D. Caurant, N. Baffier, L. Mazerolles, C. Fillet, Glass–ceramic nuclear waste forms obtained from SiO_2–Al_2O_3–CaO–ZrO_2–TiO_2 glasses containing lanthanides (Ce, Nd, Eu, Gd, Yb) and actinides (Th): study of internal crystallization, J. Nucl. Mater. 335 (2004) 14–32, https://doi.org/10.1016/j.jnucmat.2004.05.020.
[5] L. Boatner, G. Beall, M. Abraham, C. Finch, P. Huray, M. Rappaz, Monazite and other lanthanide orthophosphates as alternate actinide waste forms, in: Scientific Basis for Nuclear Waste Management, Springer, 1980, pp. 289–296.
[6] M. Kim, J. Heo, Calcium-borosilicate glass-ceramics wasteforms to immobilize rare-earth oxide wastes from pyro-processing, J. Nucl. Mater. 467 (2015) 224–228, https://doi.org/10.1016/j.jnucmat.2015.09.040.
[7] M. Kim, J. Heo, Vitusite glass-ceramics wasteforms for immobilization of lanthanide wastes generated by pyro-processing, Ceram. Int. 41 (2015) 6132–6136, https://doi.org/10.1016/j.ceramint.2015.01.035.
[8] M.A. Kim, J.H. Song, W. Um, N. Hyatt, S.K. Sun, J. Heo, Structure analysis of vitusite glass–ceramic waste forms using extended X-ray absorption fine structures, Ceram. Int. 43 (2017) 4687–4691, https://doi.org/10.1016/j.ceramint.2016.12.129.
[9] M. Kim, C.L. Corkhill, N.C. Hyatt, J. Heo, Development, characterization and dissolution behavior of calcium-aluminoborate glass wasteforms to immobilize rare-earth oxides, Sci. Rep. 8 (2018) 1–8, https://doi.org/10.1038/s41598-018-23665-z.
[10] M. Kim, M.G. Ha, W. Um, H.G. Kim, K.S. Hong, Relationship between leaching behavior and glass structure of calcium-aluminoborate waste glasses with

obtained as 199.5 kJ/mol, which indicates the energy required for the phase transformation (from this glass phase to the $LaBO_3$ crystalline phase). According to the theory of crystallization kinetics [13,28], glasses have to overcome a certain potential barrier when the glasses transform into their crystalline state, and the height of the potential barrier is defined as E_c. Therefore, the larger the E_c, the higher the potential barrier that the glass needs to overcome for the transformation [13,28]. The value of La15 (199.5 kJ/mol) is similar to or slightly smaller than 200–260 kJ/mol from the previously studied various CaO–B_2O_3–SiO_2 glass-ceramics [29]. In addition, the value is comparable to those of other wasteforms developed for the immobilization of actinide wastes; for example, 179 kJ/mol for 10 wt%- and 213 kJ/mol for 18 wt%-CeO_2-containing borosilicate glasses [13].

4. Conclusion

The thermal stability and crystallization behaviors of La_2O_3 containing B_2O_3–CaO–Al_2O_3 glass waste forms were investigated. For La15, 31% of ρ and 16% of V_m rise sharply compared to the values of La0. The glass transition temperature (T_g) was 642 °C and the crystallization temperature (T_x) was 824 °C. $LaBO_3$ phases were observed as major crystals from 780 °C by X-ray diffraction and exhibited needlelike structures by secondary electron microscopy.

various La_2O_3 contents, J. Nucl. Mater. (2020) 152331, https://doi.org/10.1016/j.jnucmat.2020.152331.

[11] W.M. Ye, Z. Zheng, B. Chen, Y.G. Chen, Y.J. Cui, J. Wang, Effects of pH and temperature on the swelling pressure and hydraulic conductivity of compacted GMZ01 bentonite, Appl. Clay Sci. 101 (2014) 192—198, https://doi.org/10.1016/j.clay.2014.08.002.

[12] C.W. Lee, S.G. Shin, Y.U. Kye, J. Heo, Evaluation of thermal stability in deep geological repository and nuclear criticality safety of spent nuclear fuel vitrified in iron phosphate glass, Ann. Nucl. Energy 136 (2020) 107055, https://doi.org/10.1016/j.anucene.2019.107055.

[13] H. Zhu, F. Wang, Q. Liao, D. Liu, Y. Zhu, Structure features, crystallization kinetics and water resistance of borosilicate glasses doped with CeO_2, J. Non-Cryst. Solids 518 (2019) 57—65, https://doi.org/10.1016/j.jnoncrysol.2019.04.044.

[14] F.G. Gibb, High-temperature, very deep, geological disposal: a safer alternative for high-level radioactive waste? Waste Manag. 19 (1999) 207—211, https://doi.org/10.1016/S0956-053X(99)00050-1.

[15] W. Lee, M. Ojovan, M. Stennett, N. Hyatt, Immobilisation of radioactive waste in glasses, glass composite materials and ceramics, Adv. Appl. Ceram. 105 (2006) 3—12, https://doi.org/10.1179/174367606X81669.

[16] J.S. McCloy, A. Goel, Glass-ceramics for nuclear-waste immobilization, MRS Bull. 42 (2017) 233—240, https://doi.org/10.1557/mrs.2017.8.

[17] H. Chen, J. Marcial, M. Ahmadzadeh, D. Patil, J. McCloy, Partitioning of rare earths in multiphase nuclear waste glass-ceramics, Int. J. Appl. Glass Sci. 11 (4) (2020) 660—675, https://doi.org/10.1111/ijag.15726.

[18] F. Wang, Q. Liao, H. Zhu, Y. Dai, H. Wang, Crystallization kinetics and glass transition kinetics of iron borophosphate glass and CeO_2-doped iron borophosphate compounds, J. Alloys Compd. 686 (2016) 641—647, https://doi.org/10.1016/j.jallcom.2016.06.066.

[19] E.A. Ferreira, F.C. Cassanjes, G. Poirier, Crystallization behavior of a barium titanate tellurite glass doped with Eu^{3+} and Er^{3+}, Opt. Mater. 35 (2013) 1141—1145, https://doi.org/10.1016/j.optmat.2012.11.006.

[20] M. Sasidharan, N. Gunawardhana, H.N. Luitel, T. Yokoi, M. Inoue, S.-i. Yusa, T. Watari, M. Yoshio, T. Tatsumi, K. Nakashima, Novel $LaBO_3$ hollow nanospheres of size 34±2nm templated by polymeric micelles, J. Colloid Interface Sci. 370 (2012) 51—57, https://doi.org/10.1016/j.jcis.2011.12.050.

[21] C.L. Chen, W.C.J. Wei, A. Roosen, Wetting, densification and phase transformation of La_2O_3-A_2O_3-B_2O_3-based glass—ceramics, J. Eur. Ceram. Soc. 26 (2006) 59—65, https://doi.org/10.1016/j.jeurceramsoc.2004.10.001.

[22] Y.S. Chang, Y.H. Chang, I.G. Chen, G.J. Chen, Y.L. Chai, Synthesis and characterization of zinc titanate nano-crystal powders by sol—gel technique, J. Cryst. Growth 243 (2002) 319—326, https://doi.org/10.1016/S0022-0248(02)01490-2.

[23] R.L. Coble, Sintering crystalline solids. I. Intermediate and final state diffusion models, J. Appl. Phys. 32 (1961) 787—792, https://doi.org/10.1063/1.1736107.

[24] M.A. Janney, H.D. Kimrey, M.A. Schmidt, J.O. Kiggans, Grain growth in microwave-annealed alumina, J. Am. Ceram. Soc. 74 (1991) 1675—1681, https://doi.org/10.1111/j.1151-2916.1991.tb07159.x|.

[25] M. Jarcho, C. Bolen, M. Thomas, J. Bobick, J. Kay, R.H. Doremus, Hydroxylapatite synthesis and characterization in dense polycrystalline form, J. Mater. Sci. 11 (1976) 2027—2035, https://doi.org/10.1007/BF02403350.

[26] R.L. Blaine, H.E. Kissinger, Homer kissinger and the kissinger equation, Thermochim. Acta 540 (2012) 1—6, https://doi.org/10.1016/j.tca.2012.04.008.

[27] H.E. Kissinger, Variation of peck temperature with heating rate in differential thermal analysis, J. Res. Natl. Bur. Stand. 57 (1956) 217.

[28] M.M. Imran, Crystallization kinetics, glass transition kinetics, and thermal stability of $Se_{70-x}Ga_{30}In_x$ (x= 5, 10, 15, and 20) semiconducting glasses, Phys. B Condens. Matter 406 (2011) 482—487, https://doi.org/10.1016/j.physb.2010.11.019.

[29] I. Shaltout, Crystallization kinetics and structure of (TeO_2-TiO_2-Fe_2O_3) glasses, J. Mater. Sci. 35 (2000) 323—329, https://doi.org/10.1023/A:1004749402741.